Structural and Multidisciplinary Optimization (2023) 66:213
https://doi.org/10.1007/s00158-023-03667-w

RESEARCH PAPER

Simultaneous optimization of topology and process parameters for laser-powder bed fusion additive manufacturing

İstemihan Gökdağ[1,2] · Erdem Acar[2]

Received: 24 April 2023 / Revised: 31 July 2023 / Accepted: 29 August 2023 / Published online: 15 September 2023

Abstract

Additive manufacturing (AM) technology is used in sectors such as automotive and aerospace, due to its advantages in producing complex and lightweight structures. However, it is necessary to reduce the total manufacturing costs for AM technology to become widespread. The topology optimization (TO) studies in the literature typically optimize only the design without taking into account the manufacturing phase or sequentially optimize the topology first and then the process parameters. On the other hand, simultaneous optimization of topology together with process parameters provides more efficient and less costly solutions. This paper describes a strategy for simultaneous optimization of topology along with process parameters of the laser-powder bed fusion (L-PBF) process. The topology, laser power, scanning speed, energy density, and yield strength are controlled by integrating the overall process–property–structure–performance relationship of the L-PBF process into the optimization. The proposed simultaneous optimization method aims to minimize the total cost function including material, manufacturing, and energy costs. Moreover, the constraint functions of the optimization include the volume fraction, the strength of the structure, and the energy density calculated according to the process parameters. The proposed method is successfully applied to three different design problems as cantilever beam, MBB beam, and L bracket, respectively. The results of different TO methods including conventional TO (compliance minimization), structural TO (similar to stress-constrained TO), and sequential process parameters and topology optimization are compared with the results of the proposed method. It is found that the proposed method provided the minimum cost results, and the obtained designs met the structural requirements.

Keywords Additive manufacturing · Simultaneous optimization · Topology optimization · Process parameters optimization · Cost minimization · Laser-powder bed fusion

1 Introduction

Additive manufacturing (AM) is a production method that generates 3D objects by adding material layer by layer (Gibson et al. 2010). AM is a more convenient method to produce complex structures, as it does not require additional cost and tools compared to conventional methods (Nazir and Jeng 2020). Additionally, since Bendsøe and Kikuchi's (1988) pioneering work, the topology optimization (TO) method, which optimizes the material distribution of the structure, has been widely preferred in the design stage. AM method also offers the ability to significantly increase fuel efficiency in many industries such as aviation (Boursier Niutta et al. 2022), space (Willner et al. 2020) and automobile (Großmann et al. 2020) by enabling the manufacture of lightweight parts that meet performance requirements and are designed with TO methods.

The structures designed by TO are not always convenient to metal AM due to various reasons such as manufacturing parameters, geometric accuracy, building direction, and anisotropy (Meng et al. 2020). Therefore, many researchers have studied to improve production quality and related costs by integrating constraints into TO (Liu et al. 2023). Since the metal AM produces the parts by melting the material, thermal issues affect the quality of the manufacturing (Craeghs

Responsible Editor: W. H. Zhang

✉ İstemihan Gökdağ
istemihan.gokdag@tai.com.tr

[1] R&D Division, Turkish Aerospace Industries Inc., Ankara, Türkiye

[2] Department of Mechanical Engineering, TOBB University of Economics and Technology, Söğütözü, Ankara, Türkiye

et al. 2012). Distortion of the structure was integrated as a constraint into TO method to improve geometric accuracy by coupling manufacturing simulation and TO (Misiun et al. 2021). A thermal constraint was integrated into TO method to control overheating during manufacturing (Ranjan et al. 2023). Moreover, supporting and overhang constraints were integrated into TO (Wang et al. 2018; Zhang and Cheng 2020).

Build orientation, support structures, and residual stress are other key factors that affect manufacturing quality and cost (Cheng et al. 2019). Building direction and topology were simultaneously optimized to get more printable designs (Chen et al. 2022). The effects of the building direction on fatigue behavior were integrated into TO method to be optimized simultaneously (Olesen et al. 2021). Additionally, since residual stress is one of the major issues in the laser-powder bed fusion (L-PBF) process, residual stress was integrated into TO to reduce deformation and defects (Allaire and Jakabčin 2018; Chen et al. 2020).

Process parameters of AM method affect the microstructure, mechanical properties, and performance of the manufactured structure (Read et al. 2015; Liverani et al. 2017). The relationship of the process parameters and performance was investigated to consider the effects of manufacturing parameters on defects and the mechanical performance of the additively manufactured parts by mapping the process parameters on the mechanical properties (Narra et al. 2023). The developed relationships were used in the simultaneous optimization of topology and process parameters to improve structural stiffness (Li et al. 2021, 2023). Many studies in the literature have focused on the mechanical performance of process parameters of AM and its application to TO methods (Liu et al. 2018). However, some of the most preventing issues to AM technology being widely used in industry are manufacturing costs, manufacturing quality, and material uncertainty (Gao et al. 2015). Build time was integrated into TO method by considering support structures to control manufacturing costs (Liu et al. 2019; Sabiston and Kim 2020) and developing process-based cost modeling (Ulu et al. 2019).

The current literature lacks a detailed description of the simultaneous optimization the topology along with the process parameters of the L-PBF to minimize manufacturing costs. The study aims to fill this gap by developing a simultaneous optimization method and applying it to various design problems. Scanning speed and laser power are selected as process parameters affecting manufacturing costs, and energy density value (one of the key factor affecting manufacturing quality and mechanical properties of the structure) is constrained during optimization. This paper is organized as follows: the production cost model, different TO methods (conventional TO, structural TO, and sequential process parameters and topology optimization), constraint aggregation technique, and the proposed TO method (simultaneous process parameters and topology optimization) are described in Sect. 2. The applications of different existing TO methods and the proposed method to three different design problems such as cantilever beam, MBB beam, and L bracket are presented in Sect. 3. In addition, the comparison of different design solutions, total costs, and manufacturing time corresponding to different TO methods are discussed in Sect. 3. Finally, the conclusions drawn from this study are presented in Sect. 4.

2 Methodology

2.1 Production cost model

The production cost of a part to be produced by AM can be broken down into two main categories: (i) material-related costs and (ii) time-related costs. The material-related costs cover the amount of material required for the design and the rate of scrapping the part when an error is encountered during production. The time-related costs cover the cost of the machine and the addition of maintenance costs to the pricing strategy, energy consumption and labor cost. Since the optimum values of the design variables used in TO determine the design of the part, they affect both the material-related and the time-related costs. Since the optimum values of the process parameters used during production directly affect the production time, they affect time-related cost items (Thomas and Gilbert 2015). Components of material-related costs are the material cost of the produced part and waste material cost, additionally, components of time-related costs are the cost of AM machine, the cost of labor, and the cost of energy to be used. Finally, the derived cost function used in this study is specified in Eq. (1) (Ulu et al. 2019).

$$\begin{aligned} Cost(\boldsymbol{\rho}, \boldsymbol{P}, \boldsymbol{V}) &= \frac{1}{(1-R)}(C_{material} + C_{time}) \\ &= \frac{1}{(1-R)}\left(C_{mat,part} + C_{mat,waste} + C_{time,machine} + C_{time,labor} + C_{time,energy}\right) \\ &= \frac{1}{(1-R)}\left[A_1 v + A_2 t + A_3 \int_{t_0}^{t} P dt + A_4\right] \\ &= \frac{1}{1-R}\left\{A_1 l_x l_y l_z \sum_i \rho_i + A_2 \frac{l_y l_z}{h} \sum_i N_i / V_i + A_3 \frac{l_y l_z}{h} \sum_i \frac{P_i N_i}{V_i} + A_4 + A_2 t_0\right\}, \end{aligned} \tag{1}$$

where R is the reject rate, $C_{material}$ is the material-related cost, C_{time} is the time-related cost, $C_{mat,part}$ is the material cost of manufactured part, $C_{mat,waste}$ is the waste material cost, $C_{time,machine}$ is the AM machine cost, $C_{time,labor}$ is the total labor cost for the produced part, $C_{time,energy}$ is the cost of energy, v is the total volume of the structure, t is the total manufacturing time, P_i is the laser power of the i^{th} element, l_x, l_y, l_z are dimensions of the hexahedral finite element, ρ_i is the artificial density value of the i^{th} element, h is the hatch distance, N_i is the number of passes to the in-layer area of the i^{th} element (cover unit distance in the x-direction), V_i is the scanning speed of the i^{th} element, and t_0 is the pre-processing

Table 1 AM machine coefficients and formulations (Ulu et al. 2019)

	Definition	Formulation
A_1	Material cost	$c_m d(1-\eta)$
A_2	Production cost	$\frac{c_i+c_m L}{LH}+c_l$
A_3	Energy cost	c_e
A_4	Scrap and pre-process energy cost	$c_m d\eta V_{env}+c_e P_0 t$

c_m is the material unit cost, d is the material density, η is the scrap rate, c_i is the investment cost, c_l is the labor cost, L is the expected life of AM machine, H is the production time per year, c_e is the electricity cost, V_{env} is the volume of the building envelope, and P_0 is the laser power during pre-processing

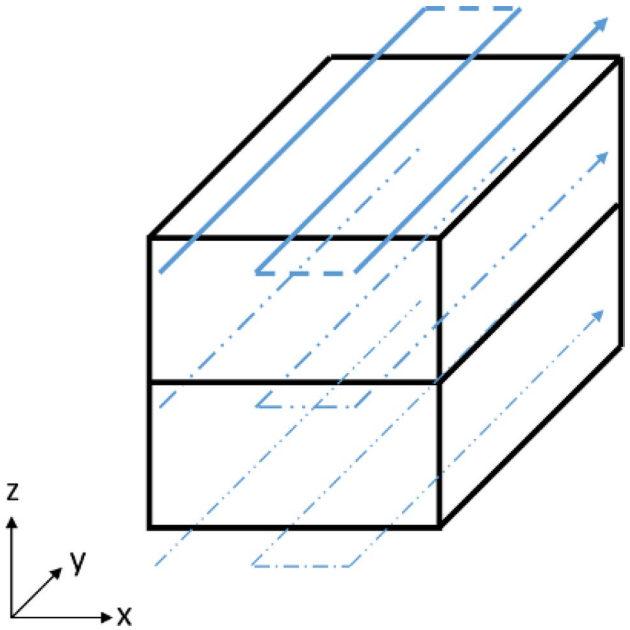

Fig. 1 Laser movement and manufacturing scheme

time before manufacturing. Additionally, the coefficients to model AM machine and formulations are given in Table 1.

The laser is traveled on the xy-plane during manufacturing, and the z-axis is determined as the build direction (see Fig. 1). According to this manufacturing scheme, the number of passes for fully melting to unit distance in the x-direction is calculated by Eq. (2), and half overlap is assumed between two melt pools.

$$N_i = 1 + G(\rho_i)\left(\frac{2l_x}{W_i} - 1\right), \tag{2}$$

where W is the melt pool width and $G(\rho_i)$ is the logistic function to adjust the number of passes of void elements. Melt pool width is a function of process parameters and it can be derived from the Rosenthal equation as given in Eq. (3) (Tang et al. 2017). Additionally, the logistic function that sets the number of passes equal to 1 for void elements is calculated by Eq. (4) (Ulu et al. 2019).

$$W \approx \sqrt{\frac{8}{\pi e}\frac{\alpha P}{dC_p V(T_m - T_0)}}, \tag{3}$$

$$G(\rho_i) = \frac{1}{1+e^{(-K(\rho_i-\rho_0))}}, \tag{4}$$

where d is the material density, T_m is the melting temperature, T_0 is the temperature far from the melt pool, α is the absorption ratio, P is the laser power, and V is the scanning speed. K is the coefficient of the logistic function to provide a smooth approximation.

The building time of additively manufactured structures is calculated as follows:

$$t_b = \int N\frac{1}{Vh}dV_{env} = \sum\nolimits_i N_i \frac{l_y}{V_i}\frac{l_z}{h}. \tag{5}$$

The effects of artificial density, laser power, and scanning speed on the cost function and its sub-cost items are demonstrated in Fig. 2. Building time and production cost increase in the range of 0–0.18 of artificial density because of the logistic function. After this range, the production cost does not change even if the artificial density increases, only the material cost goes up linearly (see Fig. 2a). On the other hand, AM process parameters (laser power and scanning speed) are inversely proportional to the production cost as given in Fig. 2b and c. It is seen that the ratio of the production cost and total cost decreases with higher laser power or scanning speed. The artificial densities are taken as 1 while calculating total costs with respect to laser power and scanning speed.

2.2 Conventional topology optimization (CTO)

In the CTO problem, the optimum design variables constrained by the volume function are calculated using compliance, which is the total strain energy of the structure, as the objective function. The CTO formulation is given in Eq. (6).

$$\begin{aligned} &\text{Find} && \boldsymbol{\rho} = [\rho_1, .., \rho_N]^T \\ &\text{Minimize} && C(\boldsymbol{\rho}) = u^T K(\boldsymbol{\rho}) u \\ &\text{Subject to} && K(\boldsymbol{\rho})u = f \\ & && v(\boldsymbol{\rho}) = \sum_{i=1}^{N} \rho_i v_i - \overline{V} \le 0 \\ & && 0 \le \rho_i \le 1 \end{aligned}, \tag{6}$$

where $\boldsymbol{\rho}$ is the artificial density vector, $C(\boldsymbol{\rho})$ is the compliance of the structure, u is the displacement vector, $K(\boldsymbol{\rho})$ global stiffness matrix, f is the external force vector, v_i is the volume of i.th element, and $\overline{V}$ is the targeted volume

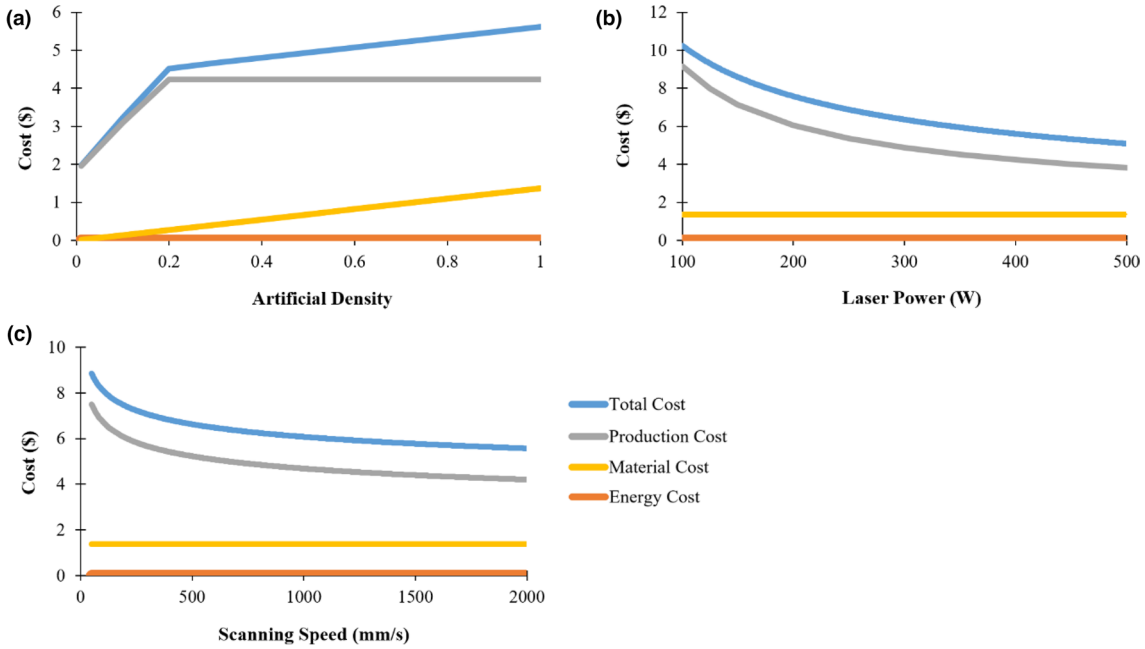

Fig. 2 Effects of parameters on the cost function (a) artificial density, (b) laser power and (c) scanning speed

value of the structure. The elastic modulus of each element is calculated using the modified SIMP method using the following equation (Sigmund 2007):

$$E_i(\boldsymbol{\rho}) = E_{min} + \rho_i^p(E_0 - E_{min}), \tag{7}$$

where E_i is the elastic modulus of each element, E_{min} is the minimum elastic modulus value used to prevent numerical singularities, p is the penalty factor, and E_0 is the elastic modulus of the material used in the design.

2.3 Structural topology optimization (STO)

Since the maximum stress or minimum compliance (strain energy) should be constrained in engineering applications, a maximum allowable compliance constraint is integrated into STO formulation. The objective function is chosen as the total cost. Thus, both deformation and strain energy calculated at each iteration is constrained by the maximum allowable compliance value and the total cost is minimized. Process parameters affect the maximum allowable compliance and they are taken as constant in STO.

$$\begin{aligned} &\text{Find} \quad \boldsymbol{\rho} = \left[\rho_1, .., \rho_N\right]^T \\ &\text{Minimize } Cost(\boldsymbol{\rho}) \\ &\text{Subject to } K(\boldsymbol{\rho})u = f \\ &\qquad \sum_{i=1}^{N} \rho_i v_i - \overline{V} \le 0 \\ &\qquad C(\boldsymbol{\rho}) - c_0^{max}(\boldsymbol{\rho}, \boldsymbol{P}, \boldsymbol{V}) \le 0 \\ &\qquad 0 \le \rho_i \le 1 \end{aligned} \tag{8}$$

where $c_0^{max}(\boldsymbol{\rho}, \boldsymbol{P}, \boldsymbol{V})$ is the maximum allowable compliance value of the structure, and it is calculated by Eq. (9) (Ulu et al. 2019):

$$c_0^{max}(\boldsymbol{\rho}, \boldsymbol{P}, \boldsymbol{V}) = \sum_{i=1}^{N} \frac{1}{k^2 E_i} v_i Y_i^T (C_0^{-1})^T Y_i, \tag{9}$$

where k is the safety factor ($k = Y_i/\sigma_i$), Y_i is the vector of yield strengths which is a 6×1 size vector, and C_0 is the unit constitutive matrix. The maximum allowable compliance is the total strain energy value of the structure which is the deformation capacity under the loading conditions. The geometry and mechanical properties of the structure affect the strain energy capacity of the design. Von-Mises stress of the structure formed during the deformation is one of the parameters in the maximum allowable compliance function, and it is used in the calculation of the safety factor of the structure. According to the Von-Mises stress results,

the yield strength of each element is adjusted by changing design variables (artificial density, laser power, and scanning speed). Thus, it is ensured that the designs remain in the safe zone in terms of structural performance by using safety factor parameter. The yield strengths of each element are calculated using the modified SIMP method similar to the elastic modulus (see Eq. (10)).

$$Y_i = Y_{min} + \rho_i^p(\sigma_y - Y_{min}), \tag{10}$$

where Y_i is the yield strength of each element, Y_{min} is the minimum yield strength value used to prevent numerical singularities, and σ_y is the yield strength of the material used in the design. Additionally, σ_y is defined as a function of process parameters (Gökdağ and Acar 2023); thus, the vector of yield strengths becomes a function of process parameters (see Eq. (11)). This yield strength model was developed for L-PBF AlSi10Mg material. There are three strengthening mechanisms, which are Hall–Petch, Orowan and dislocation hardening, determining the yield strength of AlSi10Mg.

$$\sigma_y(\mathbf{P},\mathbf{V}) = \sigma_0 + \sigma_{H-P}(\boldsymbol{P},\mathbf{V}) + \sigma_{Orowan}(\boldsymbol{P},\mathbf{V}) + \sigma_{dislocation}, \tag{11}$$

$$\sigma_0 + \frac{k}{\sqrt{0.0067(\frac{\alpha P_i}{V_i})^{0.788}}} + \frac{\varphi G b}{226.6(\frac{\alpha P_i}{V_i})^{0.5445}}(\frac{6v_{Si}}{\pi})^{1/3} + \beta M G b\sqrt{\rho_d},$$

where σ_0 is the resistance to dislocation motion, k is the strengthening coefficient, φ is the material coefficient, G is the shear modulus, b is the Burger's vector, v_{Si} is the volume fraction of Si precipitates, β is the strengthening coefficient, M is the Taylor factor, and ρ_d is the dislocation density.

2.4 Sequential Process Parameters and Topology Optimization (SePPTO)

The formulation to optimize process parameters used in the literature is stated by Eq. (12) (Ulu et al. 2019).

$$\begin{aligned} \text{Find} \quad & [\mathbf{P},\mathbf{V}] = \left[\mathrm{P}_1,..,\mathrm{P}_\mathrm{N},\ \mathrm{V}_1,..,\mathrm{V}_\mathrm{N}\right]^\mathrm{T} \\ \text{Minimize} \quad & Cost(\boldsymbol{\rho},\ \boldsymbol{P},\boldsymbol{V}) \\ \text{Subject to} \quad & K(\boldsymbol{\rho})u = f \\ & C(\boldsymbol{\rho}) - c_0^{max}(\boldsymbol{\rho},\boldsymbol{P},\boldsymbol{V}) \le 0 \\ & P_{min} \le P_i \le P_{max} \\ & V_{min} \le V_i \le V_{max} \end{aligned}, \tag{12}$$

According to Eqs. (1) and (5), which are elements of the total cost function, it is understood that the building time, the production cost, and the total cost are reduced by increasing the scanning speed. Thus, the objective function (total cost) can be improved directly at the higher scanning speed. In addition, the yield strength increases at higher scanning speeds, thereby relieving the maximum allowable compliance constraint. If the scanning speed increases, the cost function decreases and the compliance constraint is relieved. Therefore, this variable converges to its upper limit value since there is no other constraint that prevents the increase of the scanning speed. Consequently, the laser power becomes the only design variable to be optimized. According to the study that explored the effects of process parameters on microstructural and mechanical properties of AlSi10Mg manufactured by L-PBF (Gökdağ and Acar 2023), scanning speed has an impact on microstructure and mechanical properties. Therefore, it is not reasonable for the scanning speed to converge directly to its upper limit value without any limitation. To provide a remedy, the volumetric energy density (ED) parameter representing the energy input and affecting the mechanical properties of the structures is integrated into Eq. (12) as a constraint function and Eq. (13) is obtained.

$$\begin{aligned} \text{Find} \quad & [\mathbf{P},\mathbf{V}] = \left[\mathrm{P}_1,..,\mathrm{P}_\mathrm{N},\ \mathrm{V}_1,..,\mathrm{V}_\mathrm{N}\right]^\mathrm{T} \\ \text{Minimize} \quad & Cost(\boldsymbol{\rho},\ \boldsymbol{P},\boldsymbol{V}) \\ \text{Subject to} \quad & K(\boldsymbol{\rho})u = f \\ & C(\boldsymbol{\rho}) - c_0^{max}(\boldsymbol{\rho},\boldsymbol{P},\boldsymbol{V}) \le 0 \\ & ED_{min} \le ED_i(\boldsymbol{P},\boldsymbol{V}) \le ED_{max} \\ & P_{min} \le P_i \le P_{max} \\ & V_{min} \le V_i \le V_{max} \end{aligned}, \tag{13}$$

where ED_i is the volumetric energy density of each element, and it is calculated by Eq. (14). Since design variables are chosen as laser power and scanning speed, the other parameters such as hatch distance (h) and layer thickness (t) are taken as constant while calculating the energy density of each element.

$$ED_i(\boldsymbol{P},\boldsymbol{V}) = \frac{P_i}{V_i ht}. \tag{14}$$

Recall that in the STO problem, the process parameters are taken as constant while the artificial density values of the finite elements are taken as the design variables. In the SePPTO problem, the optimum artificial density values obtained as a result of STO are taken as constant (that is the optimum topology of the design and it is considered fixed), and the optimum values of the process parameters that leads to minimum total cost are calculated. Finally, the compliance and volumetric energy density functions are constrained in the SePPTO problem.

2.5 Calculation of ED constraint function using KS (Kreisselmeier–Steinhsauser) function

The ED constraint function is needed to be calculated for each finite element. In TO, the number of local constraint functions is equal to the number of design variables. Since the number of design variables is high in TO, both the calculation of

constraint functions and their derivatives make the optimization solution inefficient (Luo et al. 2013). The most common method used to solve the problem of a large number of local constraint functions is to combine the constraints into a single global function. In the literature, KS function, P-norm, and P-mean methods are used as constraint aggregation methods (Kreisselmeier and Steinhauser 1979; Yang and Chen 1996; Duysinx and Sigmund 1998). In this study, the modified KS function with reduced numerical difficulties is used and calculated by Eq. (15) (Martins and Poon 2005).

$$KS\left(g_j(x)\right) = g_{max}(x) + \frac{1}{\rho_{KS}} ln\left[\sum_j^{n_g} e^{\rho_{KS} g_j(x) - g_{max}(x)}\right], \tag{15}$$

where g_j is the calculated energy density functions, ρ_{KS} is the aggregation parameter, and g_{max} is the maximum value of constraints. The derivative of the aggregated ED constraint function with respect to design variables is calculated as stated in Eq. (16) (Raspanti et al. 2000).

$$\begin{aligned}\frac{\partial KS}{\partial x} &= \frac{\partial g_{max}(x)}{\partial x} + \frac{\sum_{j=1}^{n_g}\left[e^{\rho_{KS}(g_j - g_{max})}\left(\frac{dg_j}{dx} - \frac{dg_{max}}{dx}\right)\right]}{\sum_{i=1}^{n_g} e^{\rho_{KS}(g_j - g_{max})}} \\ &= \frac{\sum_{j=1}^{n_g}\left[e^{\rho_{KS}(g_j)}\left(\frac{dg_j}{dx}\right)\right]}{\sum_{i=1}^{n_g} e^{\rho_{KS}(g_j)}}.\end{aligned} \tag{16}$$

In this study, energy density constraints are aggregated using the modified KS function. Aggregated ED function and its derivatives are calculated by Eq. (17) and Eq. (18), respectively. Since the ED constraint function has both lower and upper bounds, calculations are performed using a separate KS function for all bounds.

$$\begin{aligned} KS_1\left(g_{1_i}\right) &= g_{1_{max}} + \frac{1}{\rho_{KS}} ln\left[\sum_i^{n_g} e^{\rho_{KS}(g_{1_i} - g_{1_{max}})}\right]; \\ g_{1_i} &= 1 - \frac{P_i}{ED_{min} V_i h t}; \\ KS_2\left(g_{2_i}\right) &= g_{2_{max}} + \frac{1}{\rho_{KS}} ln\left[\sum_i^{n_g} e^{\rho_{KS}(g_{2_i} - g_{2_{max}})}\right]; \\ g_{2_i} &= \frac{P_i}{ED_{max} V_i h t} - 1;\ g_{2_i} = \frac{P_i}{ED_{max} V_i h t} - 1; \end{aligned} \tag{17}$$

$$\begin{aligned}\frac{\partial KS_1\left(g_{1_i}\right)}{\partial V} &= \frac{\sum_{i=1}^{n_g}\left[e^{\rho_{KS}\left(g_{1_i}\right)}\left(\frac{P_i}{ED_{min} V_i^2 h t}\right)\right]}{\sum_{i=1}^{n_g} e^{\rho_{KS}\left(g_{1_i}\right)}};\ \frac{\partial KS_2\left(g_{2_i}\right)}{\partial P} \\ &= \frac{\sum_{i=1}^{n_g}\left[e^{\rho_{KS}\left(g_{2_i}\right)}\left(\frac{1}{ED_{max} V_i h t}\right)\right]}{\sum_{i=1}^{n_g} e^{\rho_{KS}\left(g_{2_i}\right)}},\end{aligned} \tag{18}$$

where $g_{1_{max}}$ is the maximum value of the g_{1_i} function and $g_{2_{max}}$ is the maximum value of the g_{2_i} function.

2.6 Simultaneous process parameters and topology optimization (SiPPTO)

It is advantageous to optimize the process parameters and topology simultaneously while finding the minimum value of the total cost. In AM process, the laser power and scanning speed affect the microstructure and mechanical properties of the structure. The yield strength of L-PBF AlSi10Mg material decreases at low scanning speed and is inversely proportional to laser power (see Fig. 3a). Process mapping of L-PBF AlSi10Mg is given in Fig. 3b, and it is shown that the same energy density (constant P/V ratio) causes same microstructural properties and same yield strength value (Gökdağ and Acar 2023).

The formulation of the SiPPTO problem, which aims to find the optimum values of three design variable vectors (artificial density, laser power, and scanning speed for each element) simultaneously, is given in Eq. (19).

$$\begin{aligned} &\text{Find} \quad [\boldsymbol{\rho}, \boldsymbol{P}, \boldsymbol{V}] = \left[\rho_1, .., \rho_N, P_1, .., P_N, V_1, .., V_N\right]^T \\ &\text{Minimize } Cost(\boldsymbol{\rho}, \boldsymbol{P}, \boldsymbol{V}) \\ &\text{Subject to } K(\boldsymbol{\rho})u = f \\ &\qquad \sum_{i=1}^{N} \rho_i v_i - \overline{V} \le 0 \\ &\qquad C(\boldsymbol{\rho}) - c_0^{max}(\boldsymbol{\rho}, \boldsymbol{P}, \boldsymbol{V}) \le 0 \\ &\qquad ED_{min} \le ED_i(\boldsymbol{P}, \boldsymbol{V}) \le ED_{max} \\ &\qquad 0 \le \rho_i \le 1 \\ &\qquad P_{min} \le P_i \le P_{max} \\ &\qquad V_{min} \le V_i \le V_{max} \end{aligned} \tag{19}$$

The procedure of the SiPPTO method is given in Fig. 4. According to the flowchart, firstly, the limits of the design variables, loading conditions, boundary conditions, and the properties of the material used in the design are determined. The value of the design variables (artificial density, scanning speed, and laser power) at the first iteration is estimated. The mechanical properties (elastic modulus and yield strength) of each finite element are calculated by the modified SIMP method using design variables. Finite element analysis of the complete model is performed. As a result of the structural analysis, the value of the objective function (total cost) and the values of the constraint functions (volume, compliance, and energy density) are calculated. The ED constraint is not imposed for each finite element, but it is used as a single global constraint function by integrating the KS function. Since the optimization is performed with a gradient-based optimization method,

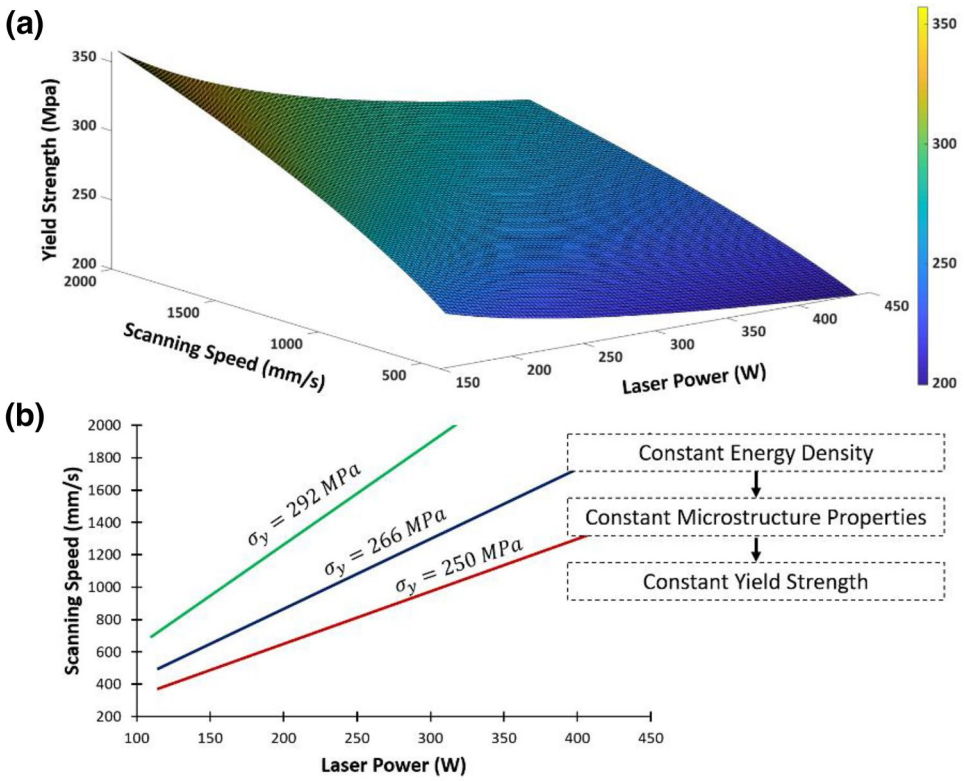

Fig. 3 Effects of process parameters on the yield strength of AlSi10Mg a) 3D plot and b) 2D plot

the derivatives of the objective and constraint functions are calculated with respect to the design variables. Filtering is performed separately for the three design variables (artificial density, laser power, scanning speed) within a certain filter radius to avoid large gradients between the adjacent elements. Thus, sharp transitions are prevented in terms of design (artificial density), scanning speed and laser power taking into account manufacturing limitations while optimizing the design variables. The values and gradient information of the calculated functions are input to the optimizer. The optimizer outputs the design variable information for the next iteration. The iterative process continues until the objective function difference between the two iterations satisfies the optimization convergence criterion. When the convergence criterion is met, the optimization is stopped and the result is accepted as optimum. As a result, using the SiPPTO method, optimum topology and process parameters (laser power and scanning speed) are obtained simultaneously, which satisfies the requirements of weight, mechanical strength and producible energy density.

The design variables, objective and constraint functions used in the topology optimization formulations discussed in this study are summarized in Table 2. CTO is the volume-constrained minimum compliance problem and the process parameters used in the production of the structure are not included in CTO. In the STO problem, an optimum topology with minimum cost and constrained by maximum allowable compliance and volume constraints is calculated. In addition, the process parameters are taken as constant in the STO problem. In the SePPTO problem, the optimum topology obtained with STO is added to the problem as input and optimum process parameters of the elements are calculated aiming for minimum cost, limited by the volumetric energy density and maximum allowable compliance constraints. Finally, in the SiPPTO problem, the minimum cost is objective and optimum artificial density and process parameters are obtained, which are constrained by volume, maximum allowable compliance, and volumetric energy density functions.

3 Numerical study

All design problems are solved using CTO, STO, SePPTO, and SiPPTO, respectively. MMA (Method of Moving Asymptotes) is used as the optimization algorithm (Svanberg 1987). The derivatives of the objective and constraint functions with respect to design variables are analytically calculated in this study to accelerate the MMA method, which is a gradient-based optimization method.

The structures are designed in CTO, STO, SePPTO, and SiPPTO using equations of (6), (8), (13) and (19), respectively. In the CTO problem, the total cost is calculated to

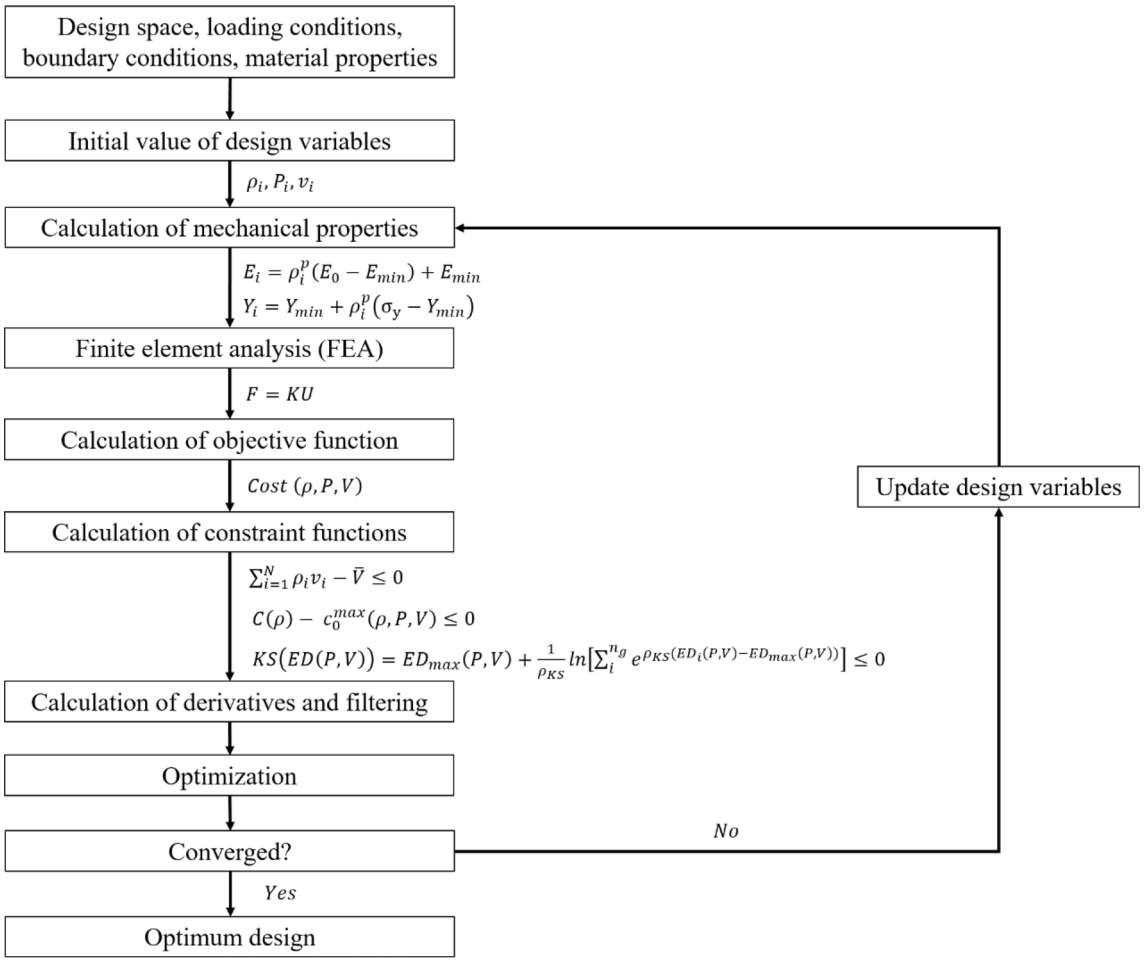

Fig. 4 Procedure of the SiPPTO method

Table 2 Comparison of different TO problems

Types of TO	Predefined Input	Design variables	Objective function	Constraint functions
Conventional topology optimization (CTO)	–	Artificial density vector	Compliance	Volume
Structural topology optimization (STO)	Process parameters	Artificial density vector	Cost	Volume, max. compliance
Sequential process parameters and topology optimization (SePPTO)	Optimum structural topology (Artificial density vector)	Process parameters vector	Cost	Energy density, max. compliance
Simultaneous process parameters and topology optimization (SiPPTO)	–	Artificial density vector, process parameters vector	Cost	Volume, energy density, max. compliance

compare with other optimization solutions although it is not the objective function of this problem. While calculating the total cost, the scanning speed and laser power are taken as 1400 mm/s and 235 W, as in the case of the STO problem. These values are chosen to remain within the feasible region of the energy density constraint, used in SePPTO and SiPPTO. In SePPTO, the design obtained with STO is used to calculate optimum process parameters so as to minimize the total cost without changing the topology. In SiPPTO, the topology and process parameters of each finite element are simultaneously optimized. The developed yield strength formulation of L-PBF AlSi10Mg with respect to

laser power and scanning speed in the literature is used in the design problems. In addition, upper and lower bounds of process parameters and ED are chosen to ensure fully melted conditions of the additively manufactured parts (Gökdağ and Acar 2023). Finally, used ED constraint functions of the optimization problems are aggregated with the KS function and integrated into the problems.

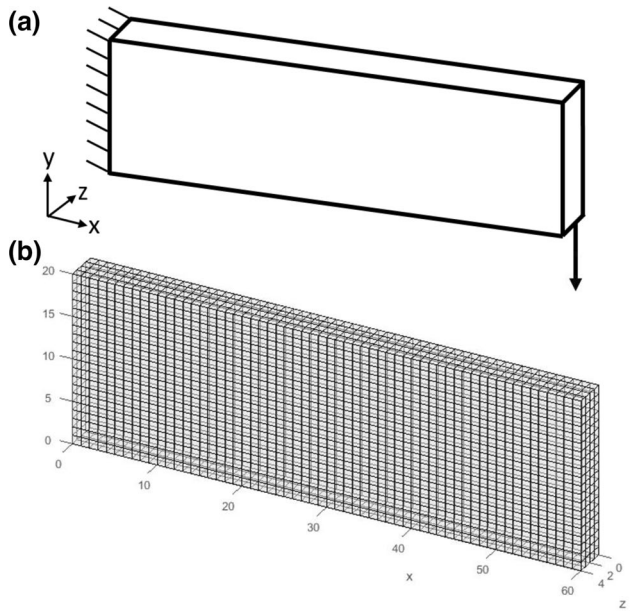

Fig. 5 The cantilever beam design setup: a) design space, loading and BCs, b) discretization

3.1 Cantilever beam design

The volume fraction (v_f) is constrained with 0.4 for this problem. The design space of the cantilever beam is given in Fig. 5. The force is applied to all nodes of the free end of the beam while the left side of the design space is constrained at all DOFs (see Fig. 5a). Finally, the design space is discretized as 60, 20, and 4 finite elements of 1mm size in the x, y, and z axes, respectively (see Fig. 5b).

The obtained optimum designs given in Fig. 6 show that the CTO design is different from the other designs. The fact that the compliance constraint is not included in the problem is determined to be the reason for this difference. On the other hand, STO design and SiPPTO design are similar to each other, with an exception that there is one strut for support close to the point where the force applied in the design obtained with the STO method. The reason for the design change is thought to be concurrent integration of the gradients of the design variables as artificial density, laser power,

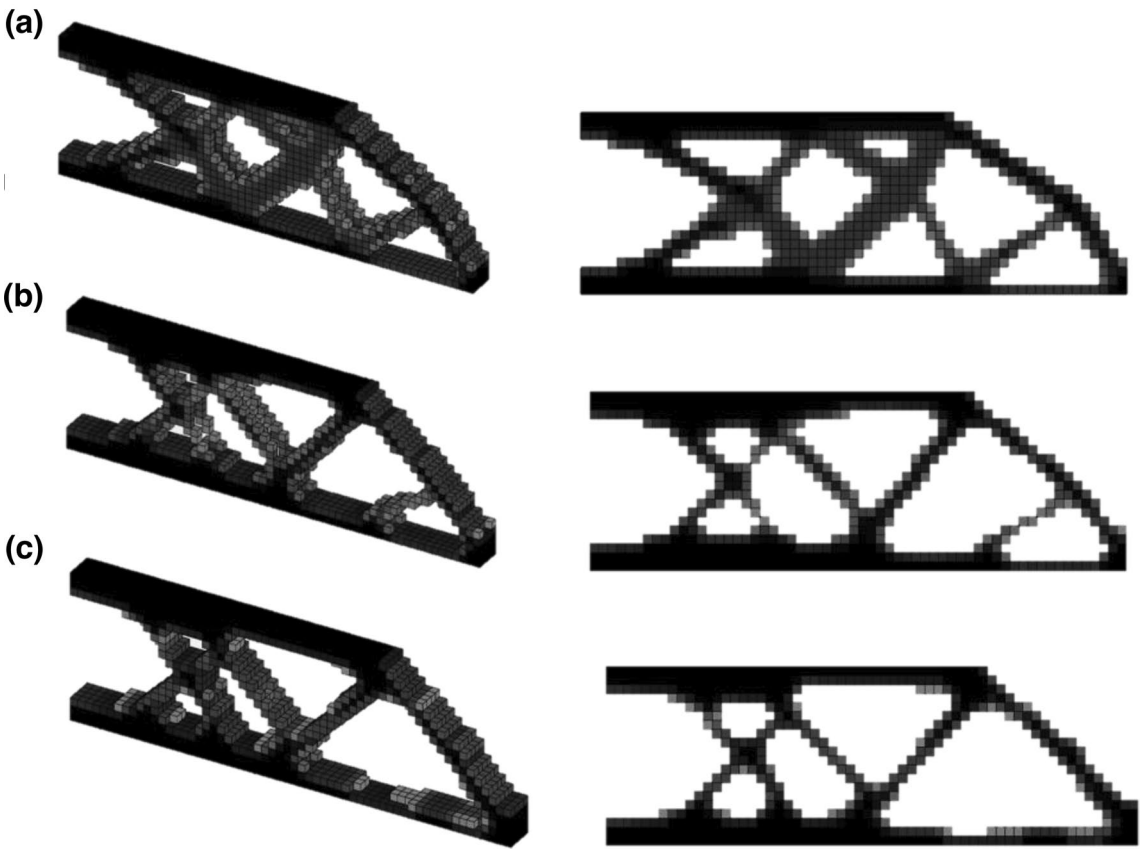

Fig. 6 Optimum cantilever beam designs: **a** CTO, **b** STO (design used in SePPTO), **c** SiPPTO

and scanning speed according to the objective and constraint functions in the SiPPTO problem.

The convergence tolerance is adjusted as 1E-03 for the total cost (objective function). According to Fig. 6, it is understood that single-node connections and the presence of gray elements can occur in the optimized designs. Finally, it is evaluated that these situations that should be avoided are the drawbacks of the SePPTO and SiPPTO methods, and it can be solved by decreasing the parameter of the convergence tolerance.

The distributions of laser power and scanning speed, normalized Von-Mises stress, yields strength, and ED of the cantilever beam results solved by SePPTO and SiPPTO are presented in Table 3. The laser power and scanning speed distributions show that the connecting beams in the middle parts of the designs should be scanned with high laser power, whereas the elements in the regions where the loading and boundary conditions are applied require lower laser power for both SePPTO and SiPPTO designs. In contrast to the laser power distribution, scanning should be performed at high speeds on the outer frame elements of the structure and at lower speeds on the middle connecting beams. These distributions of process parameters can be explained by stress and yield strength distributions. The finite elements exposed to high stress should have higher yield strength, and the relation of stress and strength is controlled by the compliance constraint function including the mechanical properties of the structure. The yield strength of the finite element is manipulated by process parameters and artificial density according to the distribution of the normalized Von-Mises stresses. In earlier work, it was determined that the yield strength increases with the faster scanning speed and decreases with the more powerful laser (Gökdağ and Acar 2023). Therefore, it is observed that the elements exposed to high Von-Mises stresses are scanned with high speed and low laser power as a result of the optimization, as expected. Additionally, it was also presented that the yield strength is inversely proportional to the ED values (Gökdağ and Acar 2023). Finally, the low ED values of the elements with high Von-Mises stress and high yield strength are explained by the ED–yield strength relationship.

The cantilever problem solved by SiPPTO method is converged in 129 iterations. The variation of the objective function, given in Fig. 7, shows that the total cost of the cantilever beam to be manufactured is decreased by 42.4%. In addition, it is considered that the reason for the increase in the total cost function between the 5^{th} and the 13^{th} iterations is a large number of design variables.

The normalized total strain energy, production time, and cost elements corresponding to the four different TO solutions are presented in Table 4 for the cantilever beam design problem. According to the strain energy results, CTO design has the lowest value since the compliance (total strain

Table 3 Optimization results of the cantilever beam problem solved by SePPTO and SiPPTO methods

	SePPTO method	SiPPTO method
a) Power distribution, b) speed distribution	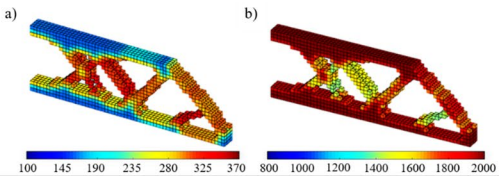	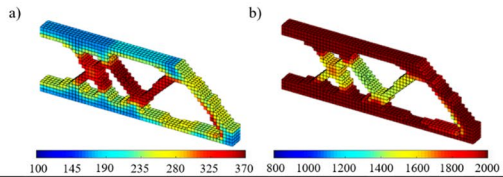
Normalized Von-Mises stress distribution	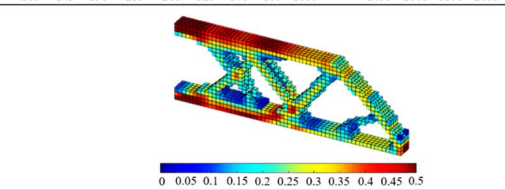	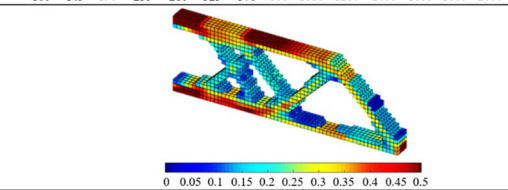
Calculated yield strength distribution a) using only process parameters, b) using both process parameters and artificial densities	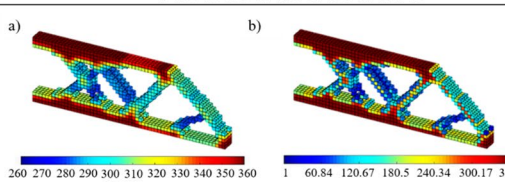	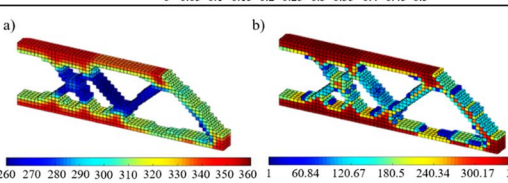
Energy density (ED) distribution	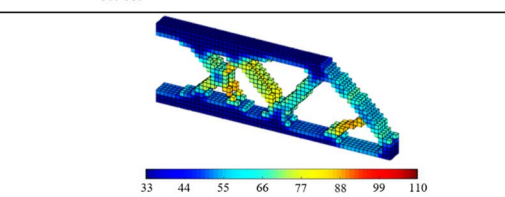	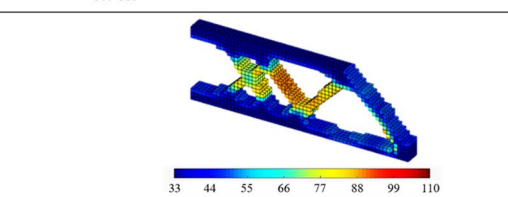

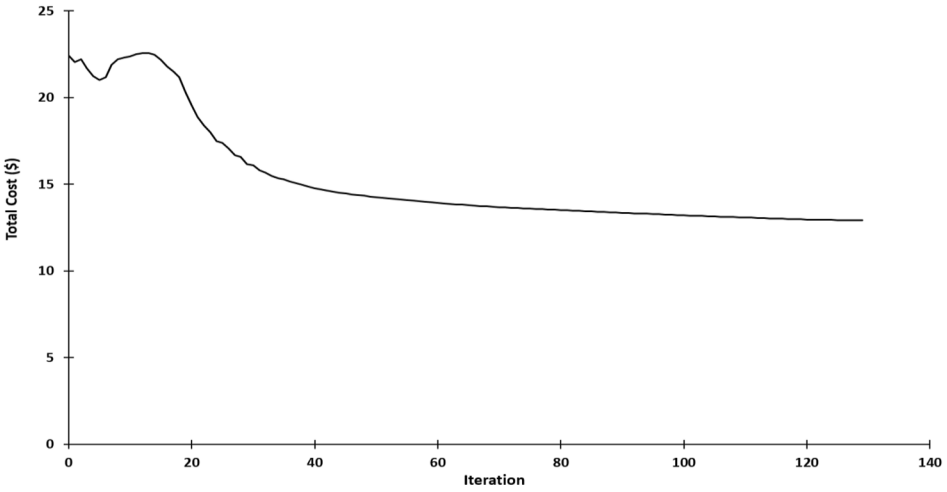

Fig. 7 Optimization history of cantilever beam design problem solved by SiPPTO method

Table 4 Strain energy, production, and cost information of cantilever beam designs

	CTO $[\rho]$	STO $[\rho]\,\vert P, V$	SePPTO $[P, V]\,\vert \rho$	SiPPTO $[\rho, P, V]$
Normalized strain energy	0.859	0.885	1	0.956
Production time (h)	0.301	0.270	0.254	0.245
Material cost ($)	0.631	0.623	0.623	0.631
Production cost ($)	15.100	13.541	12.767	12.279
Energy cost ($)	0.002	0.002	0.002	0.002
Total cost ($)	15.737	14.170	13.395	12.915
Cost saving compared to CTO (%)	-	10.0	14.9	17.9

energy) is the objective function to be minimized. STO design has the second lowest value, followed by SiPPTO and SePPTO solutions. For all solutions except CTO, designs are performed with a safety factor of 1.5. Thus, it is ensured that all structures remain on the safe side with calculating safety factor. Optimization of only the topology (with the fixed process parameters) and then the process parameters (with the design fixed) is not effective in terms of total strain energy. The reason why the total strain energy is relatively high in SePPTO and SiPPTO solutions is that these two methods do not use the same process parameters throughout the structure. Thus, they can change the process parameters to reduce the total production cost in places where the Von-Mises stress value is low (less stiffness requirement). As a result, it is understood that the SiPPTO solution provides a design that meets the structural requirements with the lowest cost.

The energy and material costs are very close for all TO solutions. Since the effect of the energy cost on the total cost is low, it does not play a significant role. The STO solution has a 10% smaller total cost compared to the CTO solution. According to the results obtained in the SePPTO problem, in which the optimum design obtained with STO is used, the total cost is reduced by 5% compared to the STO solution (14.9% total cost reduction compared to the CTO solution) through optimization of the process parameters.

In the SiPPTO solution, where both the artificial density and the process parameters are optimized simultaneously, the total cost is further reduced by 3% compared to the SePPTO solution. The total cost obtained by the SiPPTO method is reduced by 7.9% and 17.9% compared to the STO and CTO solutions, respectively. Therefore, it is understood that the SiPPTO method provides the mechanical strength requirements and least-cost result through concurrent optimization of the design and manufacturing parameters, and it can be successfully applied to small-scale design problems.

3.2 MBB beam design

The volume fraction (v_f) is limited to 0.3 for this problem. The design space of the MBB beam is given in Fig. 8. Moreover, force is applied as a nodal force on the middle of the beam while the nodes in the corners at the bottom of the y-axis are constrained at all DOFs in y and z axes (see Fig. 8a). Finally, the design space is discretized as 60, 10, and 10 finite elements of 1mm size in the x, y, and z axes, respectively (see Fig. 8b).

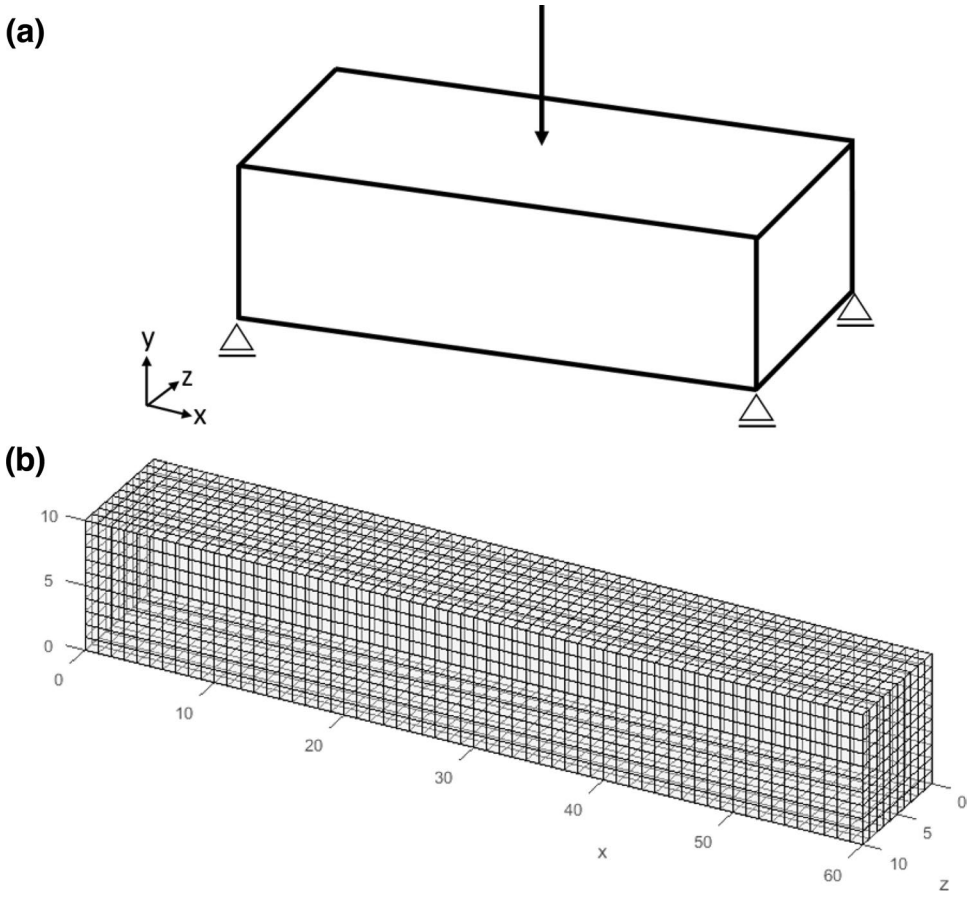

Fig. 8 The MBB beam design setup: **a** design space, loading and BCs, **b** discretization

The obtained optimum MBB designs given in Fig. 9 show that the CTO design is different from the other designs. As noted earlier, the fact that the compliance constraint is not included in the problem is determined to be the reason for this difference. Moreover, STO and SiPPTO results are similar to each other, but the method of joining the struts in the middle region with the ceiling region is the major difference. In addition, it is determined that there are differences in the thickness of the struts.

The distributions of laser power and scanning speed, normalized Von-Mises stress, yields strength, and ED of the MBB beam results corresponding to the SePPTO and SiPPTO solutions are presented in Table 5. It is seen that the finite elements in the top and bottom regions of the beam require low laser power and high scanning speed for both SePPTO and SiPPTO solutions. In particular, since the elements in the region where the force is applied are exposed to higher stress, it is determined that the elements in that region should be scanned at higher scanning speed and lower laser power. In the SiPPTO solution, it is seen that the middle region of the beam is manufactured with higher laser power compared to the SePPTO solution. The reason for the difference can be attributed to the variations of the final designs and especially the middle region of the beams. Finally, it is concluded that yield strength and ED distributions are compatible based on Von-Mises stress distributions.

The normalized total strain energy, production time, and cost elements corresponding to the four different TO solutions are presented in Table 6 for the MBB beam design problem. SePPTO design has the maximum normalized total strain energy value, followed by SiPPTO, STO, and CTO, respectively, as expected. It is seen that the energy and material costs are very close for all TO solutions. The STO solution has a 10.6% smaller total cost than the CTO solution. Since the objective function is the total cost in the STO problem, this decrease is expected behavior. Moreover, in the SePPTO problem, the optimum process parameters are calculated using the optimum design obtained from STO. According to the results of SePPTO, the total cost is reduced by 5.2% compared to STO (15.8% total cost reduction compared to the CTO solution).

In the SiPPTO solution of the MBB beam design problem, the total cost is further reduced by approximately 5%

Fig. 9 Optimum MBB beam designs: **a** CTO, **b** STO (design used in SePPTO), **c** SiPPTO

Table 5 Optimization results of the MBB beam problem solved by SePPTO and SiPPTO methods

	SePPTO method	SiPPTO method
a) Power distribution, b) speed distribution	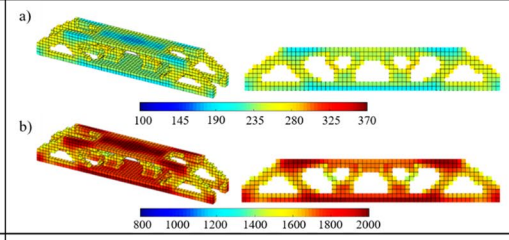	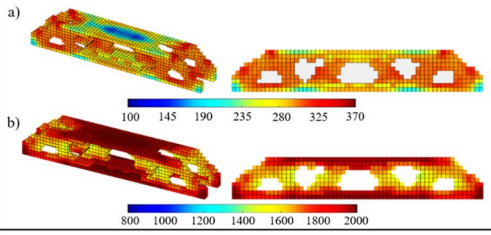
Normalized Von-Mises stress distribution	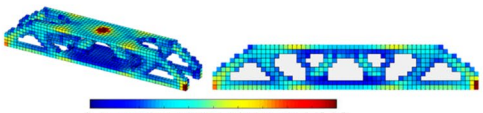	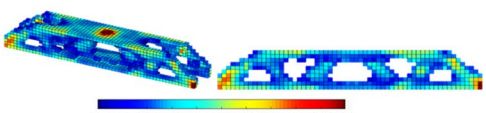
Calculated yield strength distribution a) using only process parameters, b) using both process parameters and artificial densities	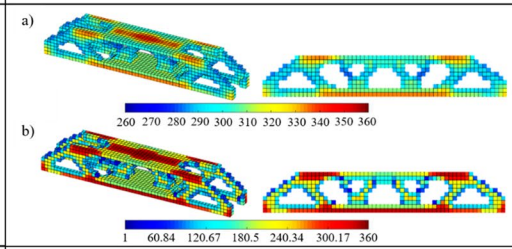	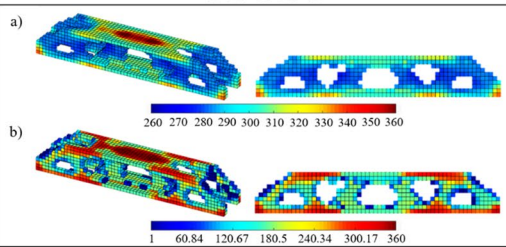
Energy density (ED) distribution	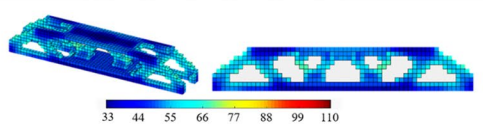	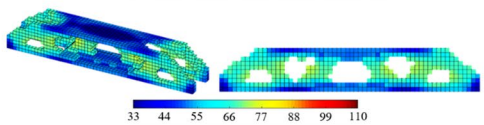

compared to the SePPTO result due to the simultaneous optimization of the design variables. The total cost of the SiPPTO is reduced by 9.9% and 20.5% compared to the STO and CTO solutions, respectively. Finally, it is understood that the SiPPTO method, which has been shown to be applicable to small-scale design problems with the cantilever beam problem, can be successfully applied to medium-size problems.

Table 6 Strain energy, production, and cost information of MBB beam designs

	CTO [ρ]	STO [ρ] |P, V	SePPTO [P, V] |ρ	SiPPTO [ρ, P, V]
Normalized strain energy	0.721	0.839	1	0.948
Production time (h)	7.35	6.53	6.13	5.77
Material cost ($)	15.97	15.97	15.97	15.84
Production cost ($)	368.77	327.84	307.83	289.92
Energy cost ($)	0.05	0.05	0.05	0.05
Total cost ($)	384.83	343.89	323.87	305.84
Cost saving compared to CTO (%)	–	10.6	15.8	20.5

3.3 L bracket design

The volume fraction (v_f) is constrained with 0.4 for this problem. The design space of the L bracket is given in Fig. 10. The force is applied to the 4th, 5th, and 6th elements in the z-axis of the bracket, and the nodes at the top point according to the y-axis are constrained at all DOFs in the x, y, and z axes (see Fig. 10a). Since the design space can be defined with a single variable along the axis for the TO setup, it is modeled as a rectangular design space using 30, 30, and 10 finite elements of 1 mm size in the x, y, and z axes, respectively (see Fig. 10b). In order to represent the design space specified in Fig. 10a, the unemployed finite elements in the x, y, and z axes are made passive by setting their artificial density variables to zero at each iteration and removed from the design space.

The obtained optimum L bracket designs given in Fig. 11 show that the solutions of the problems in which the compliance constraint function is used are similar to each other, whereas the solutions of CTO are different from the other results (as discussed in the cantilever and MBB beam design problems). Additionally, the designs of STO and SiPPTO are almost identical with only a few thickness differences identified. The reason for the thickness change is thought to be simultaneous integration of the gradients of the design variables as artificial density, laser power, and scanning speed according to the objective and constraint functions in the SiPPTO method.

The distributions of laser power and scanning speed, normalized Von-Mises stress, yield strength, and ED of the L bracket results corresponding to the SePPTO and SiPPTO solutions are presented in Table 7. According to the stress distributions, the Von-Mises stresses between the elements in the support connection of the bracket and the elements on the lower left side are calculated as high in a strip. In addition, the elements in the region where force is applied are locally exposed to higher stresses. Relatively lower stresses are calculated in the remaining elements. Since the compliance constraint is integrated into SePPTO and SiPPTO methods, the stress–strength relation is considered during the optimization. When the optimum process parameters of the SePPTO and SiPPTO solutions are investigated, it is

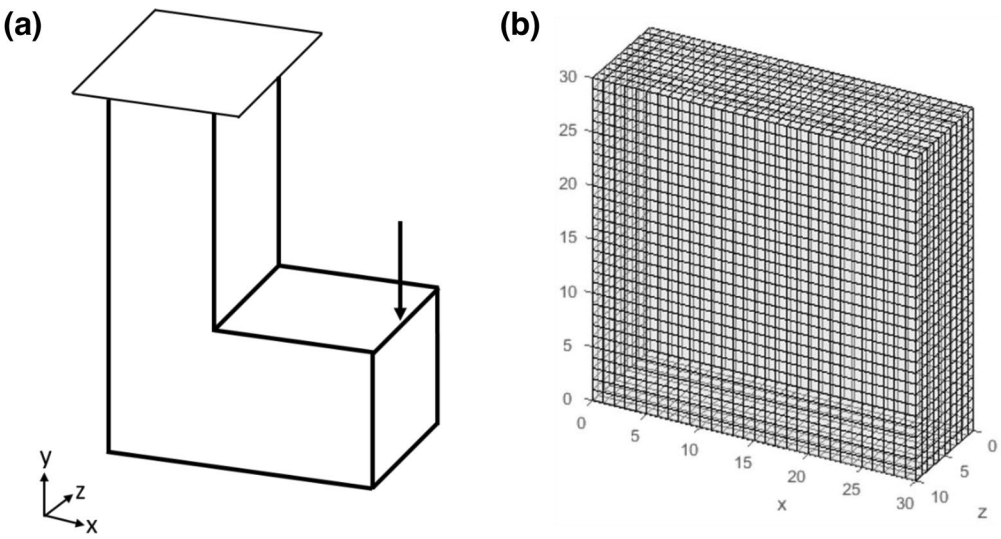

Fig. 10 The L bracket design setup: **a** design space, loading and BCs, **b** discretization

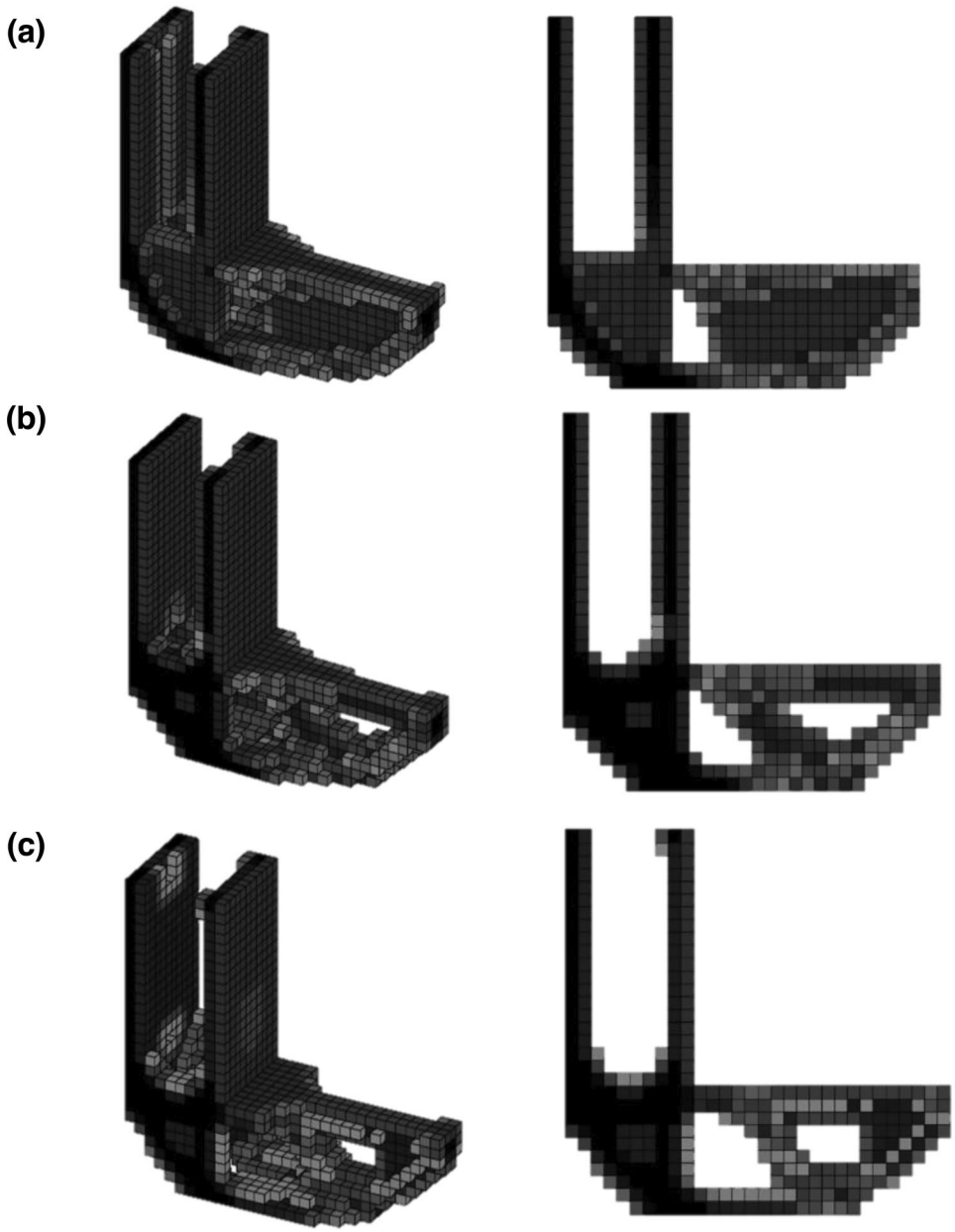

Fig. 11 Optimum L bracket designs: **a** CTO, **b** STO (design used in SePPTO), **c** SiPPTO

seen that the elements on the left of the final designs are scanned at low laser power and high speeds, while the elements in the interior of the brackets are scanned at high laser power and lower speeds for both SePPTO and SiPPTO solutions. Although the distributions of the process parameters are similar, the inner part of the bracket is manufactured at lower speed and higher laser power in the SiPPTO solution compared to the SePPTO solution. Additionally, it is seen that the finite elements exposed to high normalized Von-Mises stress have low ED values since the strength is inversely proportional to the ED value.

The normalized total strain energy, production time, and cost elements corresponding to the four different TO solutions are presented in Table 8 for the L bracket design problem. The same trend in terms of the normalized total strain energy as for the other two design problems is observed in L bracket design. On the other hand, it is seen that the energy cost can be improved when the SiPPTO method is applied to the bigger size problem, unlike other design problem solutions. The STO solution has a 5% smaller cost than the CTO solution. According to the results obtained with the SePPTO method, the total cost is reduced by 11.1% compared to the STO solution (16% total cost reduction compared to the CTO solution) through the optimization of process parameters.

In the SiPPTO solution simultaneously optimizing both the artificial density and process parameters, the total cost is reduced by 1.4% compared to the SePPTO solution.

Table 7 Optimization results of the L bracket problem solved by SePPTO and SiPPTO methods

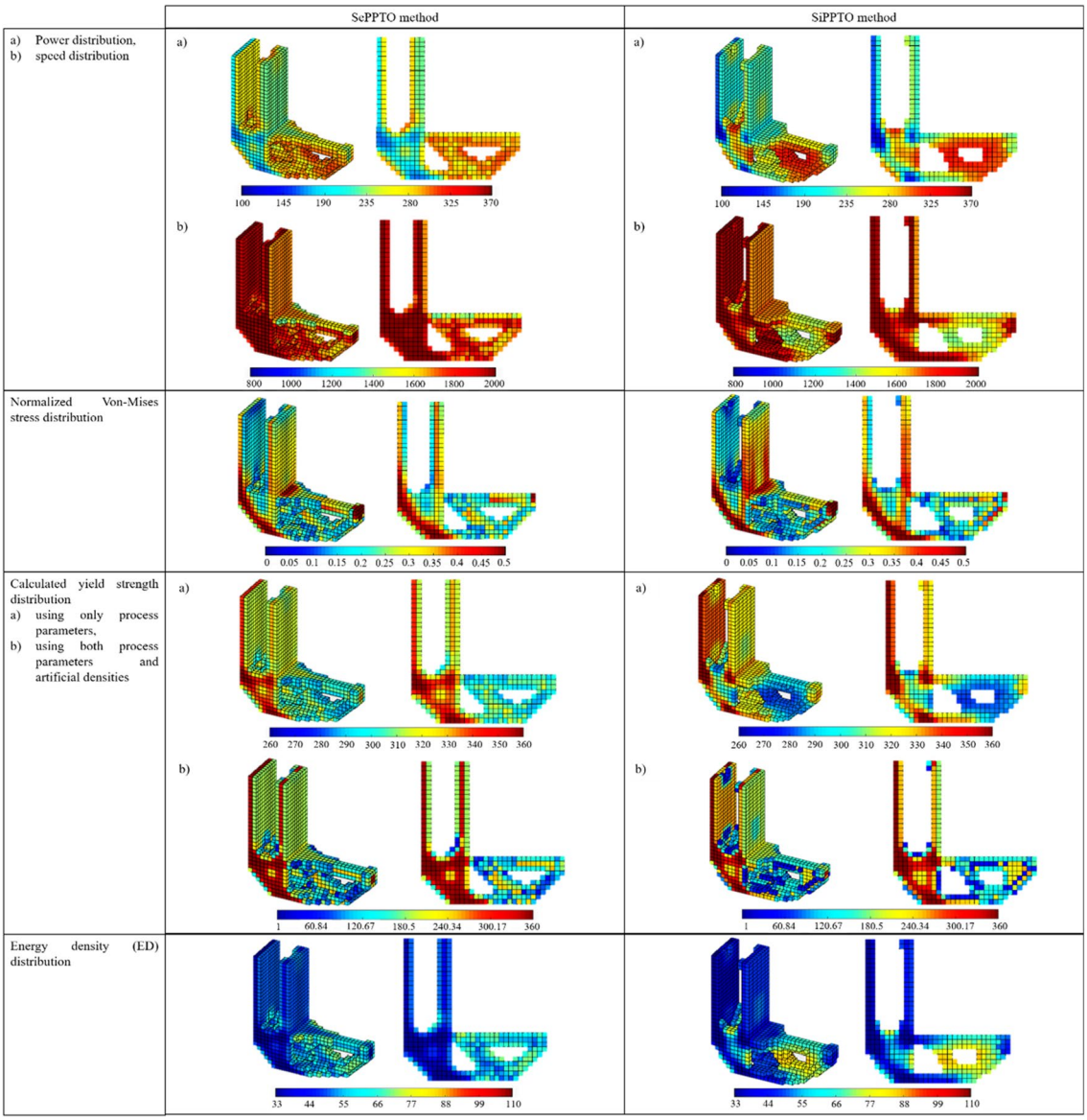

Table 8 Strain energy, production, and cost information of L bracket designs

	CTO $[\rho]$	STO $[\rho]\,\vert P, V$	SePPTO $[P, V]\,\vert \rho$	SiPPTO $[\rho, P, V]$
Normalized strain energy	0.803	0.852	1	0.939
Production time (h)	56.80	53.78	47.15	46.37
Material cost ($)	141.07	142.00	142.00	140.49
Production cost ($)	2849.88	2698.65	2365.71	2326.50
Energy cost ($)	0.41	0.39	0.38	0.35
Total cost ($)	2998.19	2847.86	2514.41	2473.64
Cost saving compared to CTO (%)	–	5.0	16.1	17.5

The total cost of the SiPPTO solution of the L bracket design problem is reduced by 12.5% and 17.5% compared to the STO and CTO solutions, respectively. Finally, it is determined that the SiPPTO method can be applied to large-scale problems such as L bracket design which is frequently used in the aerospace industry.

4 Conclusion

In this study, a procedure for simultaneous optimization of topology and process parameters (laser power and scanning speed) was comprehensively described. The laser power and scanning speed affect production time and the total cost as well as the mechanical properties of the structure. The topology of the structure impacts the mechanical strength of the design, and the process–property–performance relationship was used to correlate the mechanical strength and process parameters. The overall process–property–structure–performance relationship was developed by integrating the topology and process parameters into the maximum allowable compliance function that takes into account the mechanical strength of the structure. Moreover, the topology of the structure, laser power, scanning speed, energy density, and yield strength could be controlled by the proposed method. Thus, it was determined that manufacturing and design optimization could be concurrently performed with the proposed method. Finally, the proposed optimization method (SiPPTO) was applied to three design problems, with an increasing number of design variables, and the results of the proposed method were compared to those of the CTO, STO, and SePPTO methods.

From the results of this study, the following conclusions were drawn:

- Topological structural design and AM process design could be performed simultaneously to reduce production costs and build time.
- The proposed SiPPTO method resulted in the minimum total cost and satisfied the mechanical requirements for the three design problems investigated.
- The overall process–property–structure–performance relationship could be successfully used during the process and topology design by controlling the laser power, scanning speed, energy density, yield strength, and topology of the structure.
- The proposed optimization method (SiPPTO) was applied to the cantilever beam (small scale), MBB beam (medium scale), and L bracket designs (large scale), respectively. The number of design variables was increased while solving the design problems and it was shown that SiPPTO method was successfully applied to different scale problems
- According to the results of the three solved design problems, the total cost was reduced by 17.5–20.5% compared to the CTO solutions, 7.9–12.5% compared to the STO solutions, and finally, 1.4–5% compared to the SePPTO solutions by the proposed SiPPTO method.

The overall process–property–structure–performance relationship of the L-PBF process was developed and integrated into the proposed method with this study. In addition, the SiPPTO method was shown to be applied successfully to the design problems investigated. As the next steps, it is planned to integrate other process parameters such as hatch distance and layer thickness that affect mechanical properties into the SiPPTO method. Finally, it is planned to modify the proposed method for strut-based structures and apply it to the lattice structure designs.

Appendix

Artificial densities determine the optimum material distribution/optimum design, so, it affects the amount of material and the material cost. If the value of artificial densities increases the objective function (total cost) will increase as well as compliance constraint will relax. There is a conflict between the increasing objective function and relaxing compliance constraint and an optimization can be performed using the conflict. This mentioned optimization is formulated given in Eq. (20). The optimization formulation does not include the volume constraint and the optimization is performed for the cantilever beam design.

$$\begin{aligned}
&\text{Find} \quad [\boldsymbol{\rho},\ \boldsymbol{P}, \boldsymbol{V}] = \left[\rho_1, .., \rho_N, P_1, .., P_N, V_1, .., V_N\right] \\
&\text{Minimize } Cost(\boldsymbol{\rho},\ \boldsymbol{P}, \boldsymbol{V}) \\
&\text{Subject to } K(\boldsymbol{\rho})u = f \\
&\qquad C(\boldsymbol{\rho}) - c_0^{max}(\boldsymbol{\rho}, \boldsymbol{P}, \boldsymbol{V}) \le 0 \\
&\qquad ED_{min} \le ED_i(\boldsymbol{P}, \boldsymbol{V}) \le ED_{max} \\
&\qquad 0 \le \rho_i \le 1 \\
&\qquad P_{min} \le P_i \le P_{max} \\
&\qquad V_{min} \le V_i \le V_{max}
\end{aligned} \tag{20}$$

Optimization results are given in Fig. 12. It is shown that laser power and scanning speed of each element converged to upper bounds (Fig. 12a, b). Due to the convergence to upper bounds, yield strength and ED values of each element are constant (see Fig. 12c,d).

After the optimization, the average of artificial densities converged to 0.56. Moreover, production and cost information are listed in Table 9. According to the results, the material cost is higher than the solution with volume constraint, as expected. On the other hand, production cost and therefore total cost is lower than the original SiPPTO solution. The yield strength of the element increases with increasing scanning speed and the compliance constraint relaxes at higher scanning speed. However, yield strength is inversely proportional to laser power. It is expected that laser power decrease and scanning speed increase at the regions that should have higher yield strength. In these results, both the decrease of the total cost and the increase of the yield strength with the increasing scanning speed

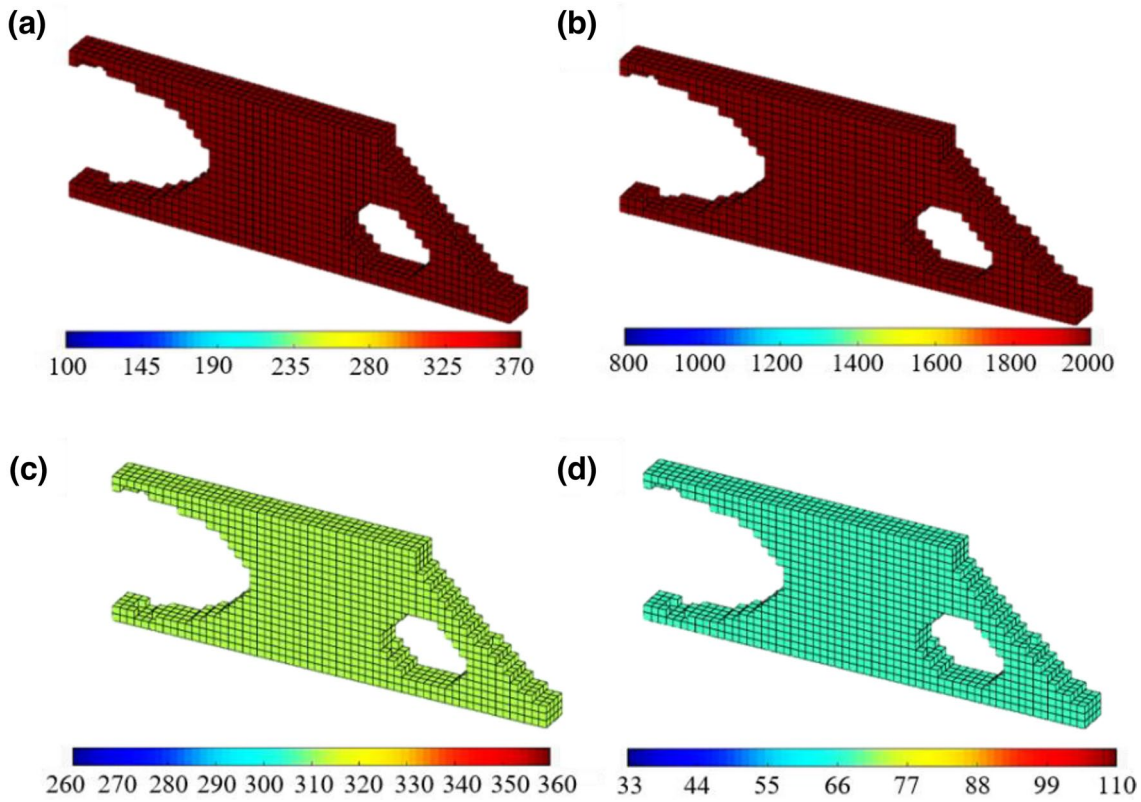

Fig. 12 Optimization results: **a** power distribution, **b** speed distribution, **c** yield strength distribution and d) ED distribution

Table 9 Production and cost information of cantilever beam designed without volume constraint

	SiPPTO [ρ, P, V]
Production time (h)	0.171
Material cost ($)	0.881
Production cost ($)	10.265
Energy cost ($)	0.002
Total cost ($)	11.151

is meaningful. However, it is unexpected that laser power converged the upper bound. Because, while decreasing the total cost with increasing laser power, the yield strength of the structure decreases. The increasing rate of the material cost is less than the increasing rate of the production cost. According to the results, it is concluded that while rising the material cost, production cost decreases radically with increasing artificial density, and therefore process parameters converge to the upper bound with the optimization formulation without the volume constraint. Therefore, it is suggested that the volume constraint function should be used in SiPPTO method.

Acknowledgements This study is a part of the project (# 5189901) supported by The Scientific and Technological Research Council of Turkey (TÜBİTAK) under the Frontier R&D Laboratory Support Program and performed in Turkish Aerospace Industries Inc. The funding provided by TÜBİTAK under Grant No. 5189901 is gratefully acknowledged.

Declarations

Conflict of interest The authors declare that they have no conflict of interest.

Replication of results The results provided herein are replicable. Interested readers may contact the corresponding author to obtain the MATLAB codes used to generate the results.

References

Allaire G, Jakabčin L (2018) Taking into account thermal residual stresses in topology optimization of structures built by additive manufacturing. Math Model Methods Appl Sci 28:2313–2366. https://doi.org/10.1142/S0218202518500501

Bendsøe MP, Kikuchi N (1988) Generating optimal topologies in structural design using a homogenization method. Comput Methods Appl Mech Eng 71:197–224. https://doi.org/10.1016/0045-7825(88)90086-2

Boursier Niutta C, Tridello A, Barletta G et al (2022) Defect-Driven topology optimization for fatigue design of additive manufacturing structures: application on a real industrial aerospace component. Eng Fail Anal 142:106737. https://doi.org/10.1016/j.engfailanal.2022.106737

Chen H, Whitefoot KS, Kara LB (2022) Concurrent build direction, part segmentation, and topology optimization for additive manufacturing using neural networks. In: Proceedings of ASME Des Eng Tech Conf 3-A: https://doi.org/10.1115/DETC2022-90050

Chen Q, Liu J, Liang X, To AC (2020) A level-set based continuous scanning path optimization method for reducing residual stress and deformation in metal additive manufacturing. Comput Methods Appl Mech Eng 360:2719. https://doi.org/10.1016/j.cma.2019.112719

Cheng L, Liang X, Bai J et al (2019) On utilizing topology optimization to design support structure to prevent residual stress induced build failure in laser powder bed metal additive manufacturing. Addit Manuf 27:290–304. https://doi.org/10.1016/j.addma.2019.03.001

Craeghs T, Clijsters S, Kruth J-P et al (2012) Detection of process failures in layerwise laser melting with optical process monitoring. Phys Procedia 39:753–759. https://doi.org/10.1016/j.phpro.2012.10.097

Duysinx P, Sigmund O (1998) New developments in handling stress constraints in optimal material distribution. In: 7th AIAA/USAF/NASA/ISSMO Symposium on Multidisciplinary Analysis and Optimization. American Institute of Aeronautics and Astronautics

Gao W, Zhang Y, Ramanujan D et al (2015) The status, challenges, and future of additive manufacturing in engineering. Comput Des 69:65–89. https://doi.org/10.1016/j.cad.2015.04.001

Gibson I, Rosen DW, Stucker B (2010) Additive manufacturing technologies. Springer, New York

Gökdağ İ, Acar E (2023) Effects of process parameters on strengthening mechanisms of additively manufactured AlSi10Mg. Mater Test 65:409–422. https://doi.org/10.1515/mt-2022-0449

Großmann A, Weis P, Clemen C, Mittelstedt C (2020) Optimization and re-design of a metallic riveting tool for additive manufacturing—a case study. Addit Manuf 31:100892. https://doi.org/10.1016/j.addma.2019.100892

Kreisselmeier G, Steinhauser R (1979) Systematic control design by optimizing a vector performance index. IFAC Proc 12:113–117

Li S, Wei H, Yuan S et al (2023) Collaborative optimization design of process parameter and structural topology for laser additive manufacturing. Chin J Aeronaut 36:456–467. https://doi.org/10.1016/j.cja.2021.12.010

Li S, Yuan S, Zhu J et al (2021) Multidisciplinary topology optimization incorporating process-structure-property-performance relationship of additive manufacturing. Struct Multidisc Optim 63:2141–2157. https://doi.org/10.1007/s00158-021-02856-9

Liu J, Chen Q, Liang X, To AC (2019) Manufacturing cost constrained topology optimization for additive manufacturing. Front Mech Eng 14:213–221. https://doi.org/10.1007/s11465-019-0536-z

Liu J, Gaynor AT, Chen S et al (2018) Current and future trends in topology optimization for additive manufacturing. Struct Multidisc Optim 57:2457–2483. https://doi.org/10.1007/s00158-018-1994-3

Liu J, Huang J, Zheng Y et al (2023) Challenges in topology optimization for hybrid additive–subtractive manufacturing: a review. Comput Des 161:103531. https://doi.org/10.1016/j.cad.2023.103531

Liverani E, Toschi S, Ceschini L, Fortunato A (2017) Effect of selective laser melting (SLM) process parameters on microstructure and mechanical properties of 316L austenitic stainless steel. J Mater Process Tech 249:255–263. https://doi.org/10.1016/j.jmatprotec.2017.05.042

Luo Y, Wang MY, Kang Z (2013) An enhanced aggregation method for topology optimization with local stress constraints. Comput Methods Appl Mech Eng 254:31–41. https://doi.org/10.1016/j.cma.2012.10.019

Martins J, Poon N (2005) On Structural Optimization Using Constraint Aggregation. In: VI World Congress on Structural and Multidisciplinary Optimization WCSMO6. Rio de Janeiro, Brasil

Meng L, Zhang W, Quan D et al (2020) From topology optimization design to additive manufacturing: today's success and tomorrow's roadmap. Arch Comput Methods Eng 27:805–830. https://doi.org/10.1007/s11831-019-09331-1

Misiun G, van de Ven E, Langelaar M et al (2021) Topology Optimization for additive manufacturing with distortion constraints. Comput Methods Appl Mech Eng 386:114095. https://doi.org/10.1016/j.cma.2021.114095

Narra SP, Rollett AD, Ngo A et al (2023) Process qualification of laser powder bed fusion based on processing-defect structure-fatigue properties in Ti-6Al-4V. J Mater Process Technol 311:117775. https://doi.org/10.1016/j.jmatprotec.2022.117775

Nazir A, Jeng JY (2020) A high-speed additive manufacturing approach for achieving high printing speed and accuracy. Proc Inst Mech Eng Part C 234:2741–2749. https://doi.org/10.1177/0954406219861664

Olesen AM, Hermansen SM, Lund E (2021) Simultaneous optimization of topology and print orientation for transversely isotropic fatigue. Struct Multidisc Optim 64:1041–1062. https://doi.org/10.1007/s00158-021-02995-z

Ranjan R, Chen Z, Ayas C et al (2023) Overheating control in additive manufacturing using a 3D topology optimization method and experimental validation. Addit Manuf 61:103339. https://doi.org/10.1016/j.addma.2022.103339

Raspanti CG, Bandoni JA, Biegler LT (2000) New strategies for flexibility analysis and design under uncertainty. Comput Chem Eng 24:2193–2209. https://doi.org/10.1016/S0098-1354(00)00591-3

Read N, Wang W, Essa K, Attallah MM (2015) Selective laser melting of AlSi10Mg alloy: process optimisation and mechanical properties development. Mater Des 65:417–424. https://doi.org/10.1016/j.matdes.2014.09.044

Sabiston G, Kim IY (2020) 3D topology optimization for cost and time minimization in additive manufacturing. Struct Multidisc Optim 61:731–748. https://doi.org/10.1007/s00158-019-02392-7

Sigmund O (2007) Morphology-based black and white filters for topology optimization. Struct Multidisc Optim 33:401–424. https://doi.org/10.1007/s00158-006-0087-x

Svanberg K (1987) The method of moving asymptotes—a new method for structural optimization. Int J Numer Methods Eng 24:359–373. https://doi.org/10.1002/nme.1620240207

Tang M, Pistorius PC, Beuth JL (2017) Prediction of lack-of-fusion porosity for powder bed fusion. Addit Manuf 14:39–48. https://doi.org/10.1016/j.addma.2016.12.001

Thomas DS, Gilbert SW (2015) Costs and cost effectiveness of additive manufacturing: A literature review and discussion. NIST Spec Publ. https://doi.org/10.6028/NIST.SP.1176

Ulu E, Huang R, Kara LB, Whitefoot KS (2019) Concurrent structure and process optimization for minimum cost metal additive manufacturing. J Mech Des. https://doi.org/10.1115/1.4042112

Wang Y, Gao J, Kang Z (2018) Level set-based topology optimization with overhang constraint: towards support-free additive manufacturing. Comput Methods Appl Mech Eng 339:591–614. https://doi.org/10.1016/j.cma.2018.04.040

Willner R, Lender S, Ihl A et al (2020) Potential and challenges of additive manufacturing for topology optimized spacecraft structures. J Laser Appl. https://doi.org/10.2351/7.0000111

Yang RJ, Chen CJ (1996) Stress-based topology optimization. Struct Optim 12:98–105. https://doi.org/10.1007/BF01196941

Zhang K, Cheng G (2020) Three-dimensional high resolution topology optimization considering additive manufacturing constraints. Addit Manuf 35:101224. https://doi.org/10.1016/j.addma.2020.101224